POLITECNICO DI TORINO
Repository ISTITUZIONALE

Estimation of PM Machine Efficiency Maps from Limited Data

(Article begins on next page)

17 October 2022

Estimation of PM Machine Efficiency Maps From Limited Data

Solmaz Kahourzade[1], Amin Mahmoudi SMIEEE [2*], Wen L. Soong MIEEE[1], Nesimi Ertugrul MIEEE[1], and Gianmario Pellegrino SMIEEE [3]

[1]School of Electrical and Electronic Engineering, University of Adelaide, Australia

[2]College of Science and Engineering, Flinders University, Australia

[3]Politecnico di Torino, Corso Duca degli, Abruzzi 24, Torino, 10129 Italy

Abstract— **This paper investigates the accuracy of the estimation of efficiency maps for permanent magnet (PM) machines using the stator resistance, *d*- and *q*-axis flux-linkages versus the corresponding axis current and the iron loss versus speed characteristic. The ultimate goal is to apply this approach to experimental measurements but this paper performs initial investigation using only finite-element data. Detailed FE data for 50-kW surface and interior PM machines is used to determine the "actual" or exact efficiency map and hence the accuracy of using approximations.**

The paper examines the effect on the torque-speed capability curve when ignoring cross-saturation effects. It also examines the modelling of the variation of iron losses as a function of load in the constant torque and power regions. A novel approach based on scaling the no-load losses as a function of load is proposed and shown to give promising results. Finite-element results from two other machines are also provided which show good correspondence.

Keywords— **Efficiency map, flux linkage, loss modeling, no-load loss, permanent magnet machine.**

I. INTRODUCTION

Efficiency maps are commonly used to graphically illustrate and compare the performance of electric machines [1, 2]. They are contour plots of the maximum efficiency on axes of torque (or power) versus speed. Efficiency maps show not only the capability envelope of the machine but also the maximum efficiency at all possible operating points [3, 4].

Efficiency maps for electrical machines can be obtained experimentally but this requires the availability of sophisticated and accurate test equipment [5]. They can also be estimated using either detailed finite element (FE) simulations or using the *d-q* equivalent circuit. An accurate calculation of the efficiency maps for electrical machines relies on detailed flux linkage and loss determination. FE analysis is considered the most precise method to calculate the efficiency map that considers the machine's non-linearities as well as the hysteresis and eddy-current losses [6]. It requires significant post-processing which includes loss data analysis for each torque-speed point in the *T-ω* plane.

The alternative method is analytical calculation based on the equivalent circuit parameters (obtained either experimentally or from FE simulations). It uses the simplified loss model which mostly considers the iron loss as a function of the speed only [7, 8]. These simplifying assumptions result in a coarse estimation of efficiency map which can be improved by considering the impacts of saturation and cross coupling [9].

A recent paper [10] has successfully improved the accuracy of efficiency map calculation by applying a scalable saturated model. The other approaches include modeling of the loss components as a function of the current and speed ($I^m \omega^n$) [11] or the torque and speed ($T^m \omega^n$) [12].

This study is a continuation of an earlier preliminary work on estimation of the iron loss only as a function of speed [13]. In [13], it was found that the estimating the iron loss only as a function of speed results in a large error especially in the field weakening region. This paper focusses on an important problem which has received limited attention in the literature: examining the accuracy of estimating efficiency maps from limited data of flux-linkage and losses. It finds that using the saturation-only flux-linkage information provides a reasonable approximation to the torque capability envelope except when the machine has a high degree of cross-saturation. The study shows that the variation of the iron and magnet losses with load can be modeled by scaling the no-load loss with an exponential function of load. The scaling factors and exponents show reasonable consistency for the same machine type in both the constant torque and constant power regions.

The proposed estimation approach is more important for experimental testing but can also be applied to FE analysis. In this paper the proposed approach is investigated using the detailed FE analysis results for example 50-kW surface and interior PM machines. The advantage of this approach is that it allows an accurate comparison between the actual (exact) efficiency map predicted by using the full set of FE analysis results and the estimated efficiency map using the equivalent circuit parameters extracted from the same FE analysis data. This allows the effects of approximations to be clearly identified. To show the suitability of the approach in this paper for a range of electrical machines (different power ratings, rotor geometries, and winding configurations), the proposed method is verified for another two different machines.

This paper is organized as follows: Section II includes the theoretical background about efficiency maps and how they are obtained using the FE calculation or experimental testing. Section III introduces the studied 50-kW SPM and IPM machines. Section IV examines the effect of flux-linkage approximations on the efficiency map of machines. Section V addresses modelling the iron loss as not dependent on load using the open-circuit, short circuit and no-load versus speed data. Section VI examines modeling the iron as a function of both load and speed. The effect of flux and iron loss estimation

on the efficiency map is compared with the exact results. Section VII shows the iron loss modeling results from two other machines types to investigate the generality of the proposed approach.

II. THEORETICAL FRAMEWORK

The efficiency map shows the maximum machine efficiency at a given torque/speed point that satisfies the machine constraints including voltage limit (usually set by the power converter DC bus voltage) and current limit (usually set by the machine/inverter thermal limits) (see Fig. 1a). Brushless PM machines normally use d- and q-axis current control to achieve smooth torque control and fast dynamic response. For a given speed, all combinations of I_d and I_q which produce the required torque (see Fig. 1b) and are compatible with both voltage and current constraints are considered (see Fig. 1c). Among these, the I_d and I_q combination resulting in the highest efficiency (lowest loss) is chosen (see Fig. 1d) to produce a single point on the efficiency map.

A. Exact Efficiency Map from Detailed FE Analysis

The efficiency map of PM machines can be calculated by using FE analysis based on sinusoidal current excitation to obtain maps of the d- and q-axis flux-linkages and iron and magnet loss as a function of the d- and q-axis currents: $\lambda_d(I_d, I_q)$, $\lambda_q(I_d, I_q)$ and $P_{fe}(I_d, I_q)$ at a given speed [6]. The effect to the variation of flux-linkage and losses with rotor position was included. It is also necessary to have the stator resistance R_s. For the flux-linkages, taking into account cross-saturation effects using $\lambda_d(I_d, I_q)$ and $\lambda_q(I_d, I_q)$ rather than the simpler saturation-only models, $\lambda_d(I_d)$ and $\lambda_q(I_q)$, allows improved accuracy for machines with high degrees of stator cross-saturation.

The iron loss, $P_{fe}(I_d, I_q)$, also includes the rotor magnet losses and includes the first 30 harmonics. The speed dependence is obtained by scaling the stator/rotor hysteresis and eddy-current loss terms separately as a function of speed to obtain $P_{fe}(I_d, I_q, \omega)$. For the iron losses, normally hysteresis loss is more important at lower speeds, while eddy-current loss is more important at higher speeds. It should be noted that as FE results were used these do not include any mechanical (bearing friction and windage) losses. The net torque for a motor as a function of I_d, I_q and ω is found using,

$$T = \frac{mp}{2}\left[\lambda_d I_q - \lambda_q I_d\right] \tag{1}$$

where m is the number of phases and p is the number of pole-pairs. The d- and q-axis voltages as a function of I_d and I_q are given by,

$$V_d = -\omega\lambda_q + I_d R_s \tag{2}$$

$$V_q = \omega\lambda_d + I_q R_s \tag{3}$$

The total loss as a function of I_d and I_q is given by the sum of the copper and iron losses,

$$P_{loss} = m(I_d^2 + I_q^2)R_s + P_{fe} \tag{4}$$

To determine the efficiency map, for each operating point defined as (T, ω), the value of (I_d, I_q) is found which produces the desired torque T from (1) while minimizing the losses in (4) and not exceeding the rated current (I_0) or voltage (V_0),

$$\sqrt{I_d^2 + I_q^2} = I \le I_0 \quad \text{and} \quad \sqrt{V_d^2 + V_q^2} = V \le V_0 \tag{5}$$

From these results the maximum efficiency as a function of (T, ω) can be found,

$$\eta = \frac{T\omega}{T\omega + P_{loss}} \tag{6}$$

This maximum efficiency for a given operating point is normally shown as a contour plot on the torque-speed plane and is called the efficiency map.

B. Experimental Parameter Measurements

The proposed approach is aimed at application to experimental testing, thus while this paper only uses simulation results, it is useful to briefly discuss the experimental test processes as the method will be simulated using FE results in this paper.

Experimental measurements can be performed to obtain both the flux-linkage and the copper and iron loss parameters. For the flux-linkage, $\lambda_d(I_d, I_q)$ and $\lambda_q(I_d, I_q)$ can be obtained using rotating tests by controlling I_d and I_q with an inverter and measuring the resultant fundamental machine d- and q-axis voltages/flux-linkages.

It is often preferable to use simpler stationary tests of flux-linkage that can only include saturation effects: $\lambda_d(I_d)$ and $\lambda_q(I_q)$. A stationary test needs to be combined with an open-circuit test to obtain the back-emf and hence d-axis magnet flux-linkage $\lambda_d(I_d=0, I_q=0)$. A further approximation is to model the machine with constant values of d- and q-axis inductance L_d and L_q,

$$\lambda_d = \lambda_m + L_d I_d \quad \text{and} \quad \lambda_q = L_q I_q \tag{7}$$

The copper loss is determined by the stator resistance, R_s. The copper loss for a given operating point (T,ω) is sensitive to the accuracy of the flux-linkage characteristics as these determine the torque for a given (I_d, I_q) combination.

For the iron and mechanical losses, it is possible to measure $P_{fe}(I_d, I_q, \omega)$ from rotating tests with an inverter and calculating the iron loss as the difference between the electrical input power and the mechanical output power after subtracting the stator copper losses using the measured stator current. It is however often preferable to use simpler and quicker tests to measure the iron loss in different situations as a function of speed only. The
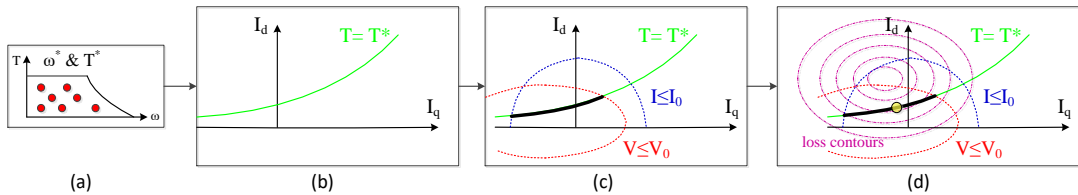

Fig. 1 Efficiency map calculation process: (a) T-ω combinations required to obtain the efficiency map, (b) combinations of I_d-I_q to produce the required torque, (c) voltage and current constraints with feasible operating points as a thick black line, (d) the I_d-I_q combination with the highest efficiency (circle)

three cases examined in this paper are two generating cases, open-circuit and short-circuit, and one motoring case, no-load.

For the generating tests, the machine is rotated using a drive machine and its iron losses found as a function of speed under open and short-circuit conditions. The iron loss is given by the mechanical input power minus the stator copper loss which is found from the measured stator current (zero for the open-circuit test). In most PM machines, the short-circuit iron loss is higher than the open-circuit iron loss, this is because the increase of spatially-harmonic losses is greater than the reduction of fundamental loss.

For the no-load test, the machine with no load on its shaft is driven by an inverter. It requires a small q-axis current to provide power for the iron (and mechanical) losses. At low speeds the d-axis current is zero, but at higher speeds, a negative value may be required to keep the terminal voltage below its rated value in (5). The no-load loss is determined from the electrical input power to the machine minus the stator copper losses.

C. Estimated Efficiency Map Using Limited Data

This paper examines the effect of using limited FE flux-linkage and iron loss data to estimate the efficiency map compared to the exact efficiency map using the detailed FE data.

The detailed FE flux-linkage data includes cross-saturation: $\lambda_d(I_d, I_q)$ and $\lambda_q(I_d, I_q)$. The limited flux-linkage data is based on the saturation-only FE data: $\lambda_d(I_d)$ and $\lambda_q(I_q)$, or even more simply, assuming linear inductances L_d and L_q.

The detailed FE iron loss data includes the variation with d- and q-axis currents and speed: $P_{fe}(I_d, I_q, \omega)$. The limited iron loss data is the open-circuit, short-circuit and no-load loss versus speed results. The open-circuit loss $P_{oc}(\omega)$ is found using the FE calculated loss $P_{fe}(I_d, I_q, \omega)$ with I_d and I_q both set to zero. For the estimated short-circuit loss, $P_{sc}(\omega)$, I_q is set to the negative characteristic current which is the high-speed short-circuit current. The estimated no-load loss, $P_{nl}(\omega)$, is found with I_q set to zero, and I_d at the minimum negative value to satisfy the voltage constraint in (5) at each speed.

III. SPM AND IPM CASE STUDY

Two examples of 50-kW PM machines are considered in this paper, one an interior PM design (IPM) and the other a surface PM design (SPM) [14]. Both are designed for a traction application. Fig. 2 shows the cross-sections of designs and Table I summarizes their parameters. Note that these machines have not been built and so only their detailed FE results are available.

IV. FLUX LINKAGE AND TORQUE ESTIMATION

Under real operating conditions, the electrical machines show some degree of saturation and cross-saturation. Under a cross-saturation condition (which is applicable to the most general case), the d- and q-axis flux linkages are functions of both d- and q-axis currents, $\lambda_q(I_d, I_q)$ and $\lambda_d(I_d, I_q)$. Figs. 3 (a) and (b) show the d- and q-axis flux variation of the studied SPM and IPM machines as a function of the corresponding axis current, e.g. $\lambda_d(I_d)$. Due to cross-saturation, there are multiple values of

flux-linkage associated with a given axis current (grey areas). This figures also shows the maximum efficiency region (yellow areas). These plots also shows the saturation-only model (red lines), and linear model (green lines). In the saturation and linear approximations, it is important that the fluxes in these regions are as close as possible to the cross-saturation operating values.
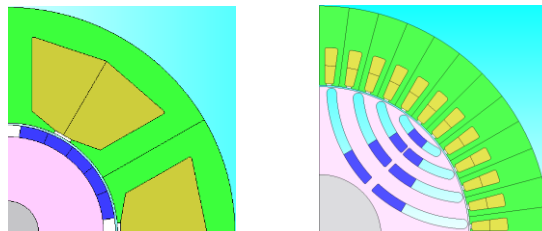

Fig. 2 Cross-sections of the two 50 kW machines (left SPM, right IPM).

TABLE I. Specifications of 50-kW, 12 kr/min Motors [14].

	#1. SPM	#2. IPM
Key Dimensions		
- stator outer diameter	216 mm	
- stack length	170 mm	
- airgap length	1 mm	0.7 mm
Material		
- steel grade	M250-35A	
- PM grade	BMN-42SH	
Design Parameters		
- poles	4	4
- stator slots	6	48
- number of turns	24	24
- copper slot fill (copper/slot area)	55%	40%
- winding type	Concentrated	Distributed
Electrical Parameters		
- max speed at continuous torque	3800 rpm	3800 rpm
- torque @ 360 A	240 Nm	164 Nm
- characteristic current (peak)	240 A	210 A
- stator resistance @130°C	20 mΩ	23 mΩ
- peak line voltage	300 V	300 V

In general, the d-axis flux linkage magnitude decreases with increasing I_q current. The effect of cross saturation is more pronounced for the SPM compared to the IPM. This is likely because the d- and q-axis flux paths share more common areas in the case of the SPM. The equivalent-circuit method is used to estimate the machine performance using the saturated and linear inductance models. In a saturation-only model, the d- and q-axis flux linkages are assumed only functions of their respective current when the other current is set to zero, that is $\lambda_d(I_d, I_q = 0)$ and $\lambda_q(I_d = 0, I_q)$.

With the highest level of approximation, the effect of saturation is ignored and machines are modelled with constant inductances as shown earlier in (7). If the flux-linkages are not heavily saturated (like λ_q for SPM and λ_d for IPM), the linear model can provide acceptable estimation of the saturated results. For the IPM q-axis flux linkage, there are two possible estimates for the linear model. The first approximation (green line) represents the unsaturated inductance while the second model (green dashed line) illustrates an approximation of the saturated inductance.
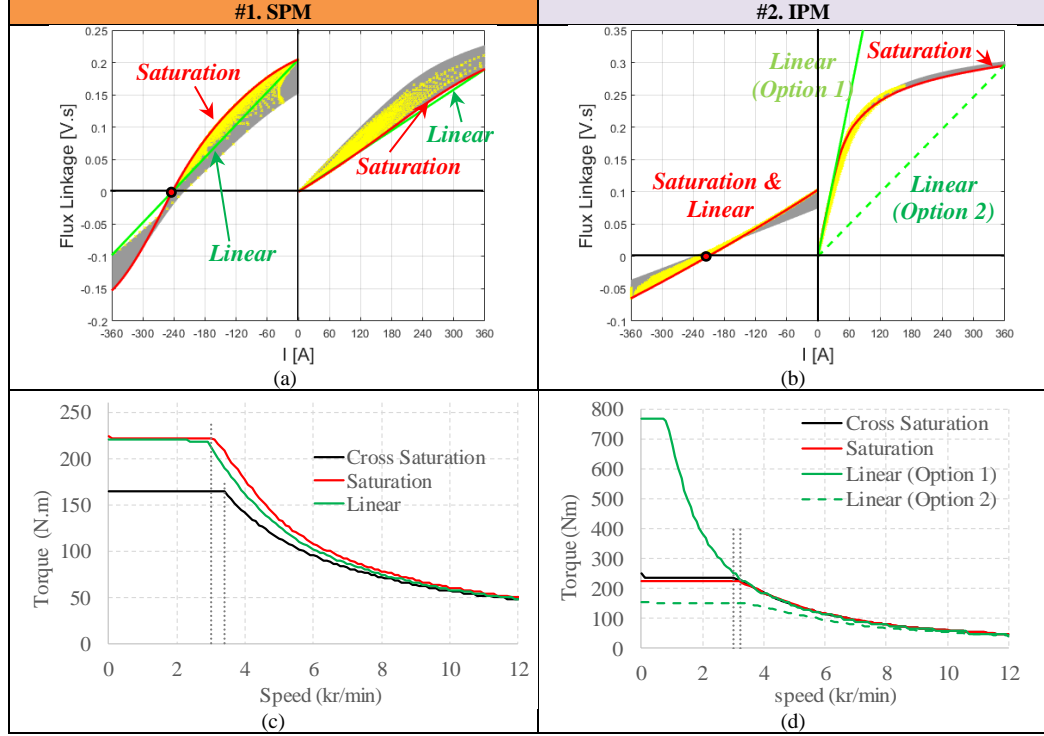
Fig. 3 Flux linkage curves and torque-speed envelopes under cross-saturation, saturation, and linear conditions. Flux-linkage curves for (a) SPM machine, (b) IPM machine. Torque speed envelope of the (a) SPM machine and (d) IPM machine.

The cross-saturation, saturation-only and linear flux-linkage models were used to predict the torque-speed capability curves in Figs. 3 (c) and (d). The SPM shows significant cross-saturation and so in the constant torque region ignoring this produces errors up to 30%. For the IPM, the lower degree of cross-saturation means the saturation-only model shows a good accuracy (about 4% error), but both the linear models have substantial errors.

In the constant power region, the machine operates with a constant voltage and a near constant current and thus the output power is much less sensitive to model flux-linkage errors. Under this condition, the current angle is adjusted to maintain the total flux-linkage inversely proportional to the speed and hence the flux-linkage errors are compensated for changes in the current angle. Thus, all the models show relatively small errors in this region that reduce with an increasing speed.

Fig. 4 shows the effect of the different flux linkage estimation models on the prediction of the copper loss in the torque-speed plane. For the SPM, it is difficult to compare the curves due to the substantial error in the capability curve in the constant torque region. The saturation-only model shows significantly better prediction than the linear model in the constant power region.

For the IPM, the saturation-only model shows good correspondence with the actual result. The presented linear model is based on second option shown in Fig. 3. It illustrates a large error as expected from the inaccurate d-axis flux linkage.

V. IRON LOSS ESTIMATION WITHOUT LOAD VARATION

The efficiency map shows the maximum efficiency for each (T,ω) operating point in the torque-speed plane. Each operating point has a corresponding copper and iron losses and the sum of them is the total loss. Note that this study is based on FE results and so does not include mechanical losses.

Fig. 5 shows the total loss (blue points) and the iron loss only (green points) at maximum efficiency operation over the entire efficiency map plotted versus speed for both the SPM and IPM machines. Given these losses generally increase with load, the loss point for each speed with the lowest loss corresponding to no load and the highest loss point corresponding to full load. The open-circuit (OC), short-circuit (SC) and no-load (NL) iron losses as a function of speed are also included in these plots for comparison. Fig. 5 shows that for the two machines, the maximum iron loss (top envelope of green iron loss points) is significantly smaller than the maximum copper loss (largest difference between the highest blue and green points for the same speed). Copper loss is roughly related to the square of torque and iron loss is roughly related to the square of speed.

Fig. 6 shows that the NL loss in the field-weakening region for the SPM is less than the OC loss while the opposite is true for the IPM. This can be explained using Fig. 6 which illustrates the iron loss of these machines at the maximum speed of 12,000 rpm (field weakening region) as a function of d-axis current with zero q-axis current. The points corresponding to OC, NL and SC operation are indicated.
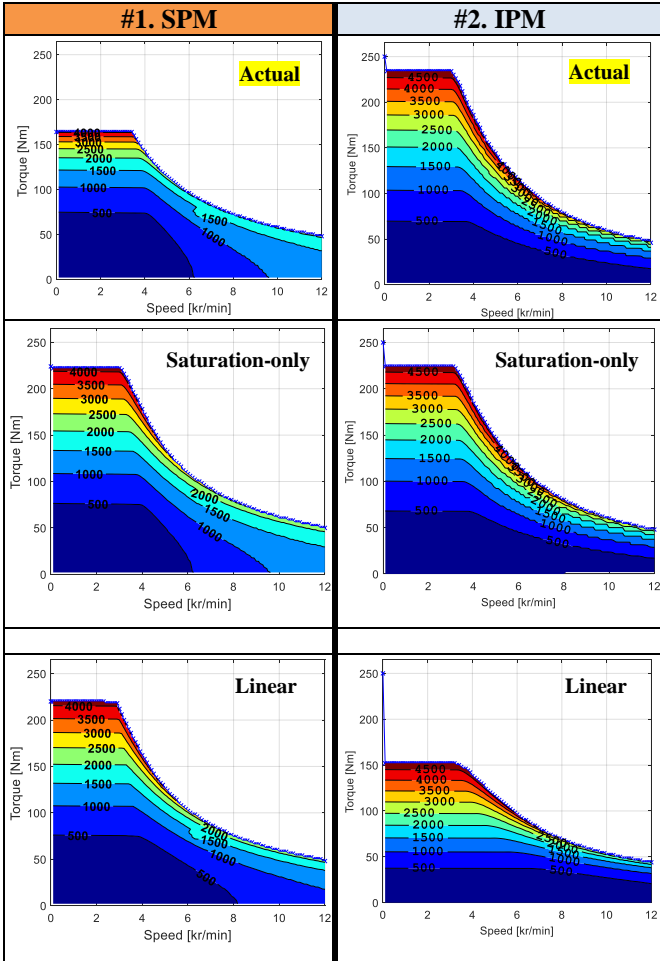
4

Fig. 4 Effect of flux-linkage estimation on copper loss. Actual and estimated copper loss values for the two motors (saturation-only and linear models).

Fig. 5 Scatter plot of iron loss and total loss versus speed overlaid by the SC, OC, and NL losses versus speed curves (top SPM, bottom IPM).

Fig. 6 Iron loss for the SPM and IPM machines as a function of d-axis current with zero q-axis current at 12,000rpm. The OC, NL and SC operating points are indicated.

Increasing the magnitude of the d-axis current in PM machines has two effects. Firstly it reduces the fundamental flux density in the machine and hence the fundamental iron loss. Secondly it creates harmonic air-gap flux densities which produce harmonic iron losses.

For the SPM, the reduction in fundamental iron loss is initially greater than the increase in harmonic iron loss producing a minimum iron loss for a value of I_d of about -120A. This effect has been used earlier for loss minimization in SPM machines [15].

For the IPM machine, the iron loss increases monotonically with d-axis current indicating the increase in harmonic iron loss exceeds the reduction in fundamental iron loss.

The SC losses are generally larger than the OC losses and for the two machines are about two to three times larger.

For the two machines, the average iron loss under load is best approximated by the OC loss for the SPM and the SC loss for the IPM. Fig. 7 shows the iron loss contour maps on axes of torque and speed and compares the exact case with estimates based on iron loss variation with speed only (OC, SC and NL). It also shows an improved approximation obtained by scaling the NL results with load which will be explained in the next
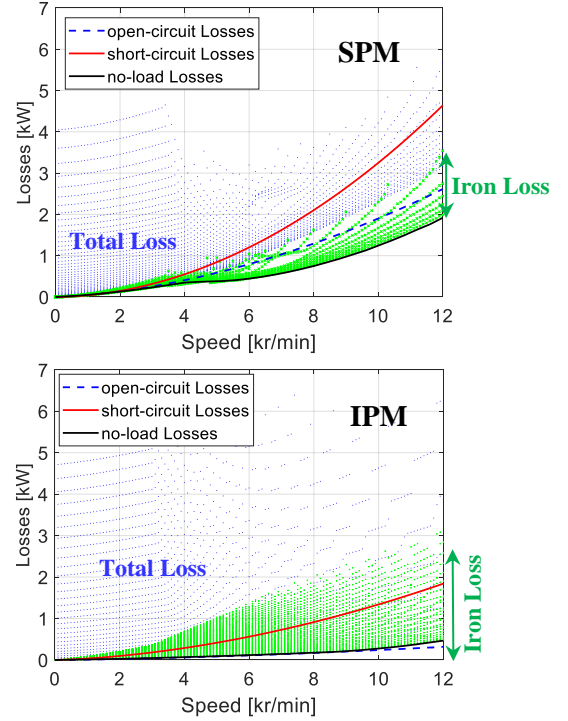
section. A consistent contour scale for the results of each machine is used to allow comparison.

Fig. 7 Exact and estimated iron loss contour plots of the SPM and IPM motors.

The differences in the iron loss are most evident in the constant power region where the losses are higher. The IPM shows a greater variation of iron loss with load than the SPM. As was observed from Fig. 7, the OC loss better approximates the average loss for the SPM while the SC loss is better for the IPM, however neither is particularly satisfactory at higher speeds.

VI. MODELING IRON LOSS VARIATION WITH LOAD

The previous section showed that using the OC, SC, and NL loss results do not provide an acceptable estimation of the iron loss. Therefore, this section investigates modelling the iron loss variations with the load.

A. Loss Analysis According to the Operation Region

Fig. 8 shows plots of the iron loss at maximum efficiency along lines of constant speed as a function of torque (row 1) and power (row 2) for the SPM and IPM machines. The blue lines represent the constant torque region and the red lines the constant power region. As expected, in the curves plotted against load torque, the constant torque lines all have a similar maximum torque. In the curves plotted against load power, for the SPM only, the constant power lines have a similar maximum power.

Fig. 8 Iron loss variation in the constant torque and constant power region versus torque and power, and effect of normalising the losses by the NL losses as a function of torque and power.

The iron loss at zero torque or power corresponds to the NL iron loss and Fig. 8 shows that the iron loss increases smoothly with both load torque and power, and also speed. There is a minor irregularity in the SPM constant power curves (in red) at around 70Nm/50kW; this is likely due to numerical errors.

B. Normalizing the Iron Loss

By studying the results in the first two rows of Fig. 8, it appears that within the constant torque and power regions, the curves for each speed have similar a shape and may be scaled versions of one another. To test this, the curves for each speed are normalised based on the NL losses at the same speed and the results are shown in rows 3 and 4 of Fig. 8 for the SPM and IPM machines. The NL losses were chosen as they provide the best match of the losses at zero output power.

The IPM constant torque curves have the closest match (smallest divergence), followed by the SPM constant torque and power curves, with the IPM constant power curves having the poorest match (largest divergence).

C. Finding Correct Function for Scaling the NL losses

It is proposed to represent the iron loss variations with load using a power law $y(x) = x^n$. Fig. 9 shows the graphs with different guesses for the exponent n. For instance in the constant torque region for the SPM, T^2 and T^4 are used while for the IPM, $T^{1/2}$ and $T^{1/3}$ are compared. For the graphs with the best fit, e.g. T^4 for the SPM, a black line shows the linear function used for the fit.

Based on the above results, it was found that the iron loss at maximum efficiency can be estimated by scaling the NL loss $P_{fe-NL}(\omega)$ as a function of load torque T and power P as follows for the constant torque and power regions, respectively,

$$P_{fe}(\mathrm{T}, \omega) = P_{fe-NL}(\omega) \times \left[1 + (K_T - 1)\left(\frac{T}{T_0}\right)^{n_T}\right] \quad (8)$$

$$P_{fe}(\mathrm{P}, \omega) = P_{fe-NL}(\omega) \times \left[1 + (K_P - 1)\left(\frac{P}{P_0}\right)^{n_P}\right] \quad (9)$$

where T_0 and P_0 are the rated torque and rated power, n_T and n_P the exponents for constant torque and constant power regions

and K_T and K_p, the scaling factors representing the ratios of the full-load to no-load iron loss for each region.

The loss contour map obtained from the scaled NL losses has been presented earlier in Fig. 7. Comparing these losses against the actual loss shown also in Fig. 7 illustrates a good correspondence between these results. The discontinuity in the contours in the scaled NL loss estimate at the rated speed is due to the use of different fitting functions in the constant torque and constant power regions.

D. Comparison of Exact and Estimated Efficiency Maps

Fig. 10 compares the exact efficiency map with the estimated efficiency maps using the saturation-only flux linkage model as well as iron loss model as only a function of speed based on the scaled no-load loss.

First consider the SPM. Case 1 shows the exact efficiency map. Case 2 shows that the saturation-only flux-linkage model over-estimates the low speed torque capability as this machine has a high degree of cross-saturation. Case 3 shows using the iron loss as only a function of speed introduces errors in the constant power regions which cause small changes particularly in the efficiency contours as they approach the capability limit. In this region, Case 4 shows a significant improvement versus Case 3 and is much closer to Case 2 which uses the exact iron loss. Comparing Case 2 and 4 shows that the scaled-NL loss method predicted the efficiency map by a maximum of 1% error which only existed in the low torque region.

For the IPM, as the machine has a low level of cross-saturation, the effect of using the saturation-only flux-linkage model is negligible and thus the Case 2 and 1 results are similar. In Case 3, using the iron loss only as a function of speed significantly affects the accuracy of the values and shapes of the efficiency contours in the constant power region. Comparing Case 4 with Case 3 and 1, shows using the scaled NL loss produces a generally better efficiency map estimate in the constant power region though the peak efficiency is over-estimated by about 1%. Note that the use of different fitting functions in the constant torque and constant power regions
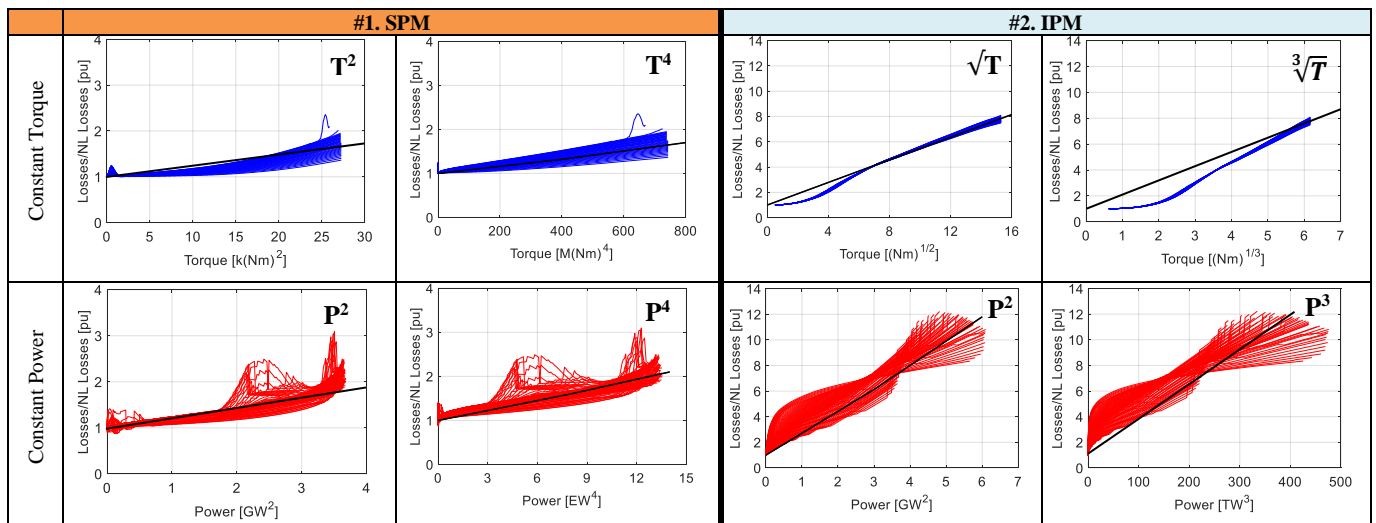

Fig. 9 Selection of the best exponent for modelling the ratio of iron loss to no-load loss versus load torque and power.

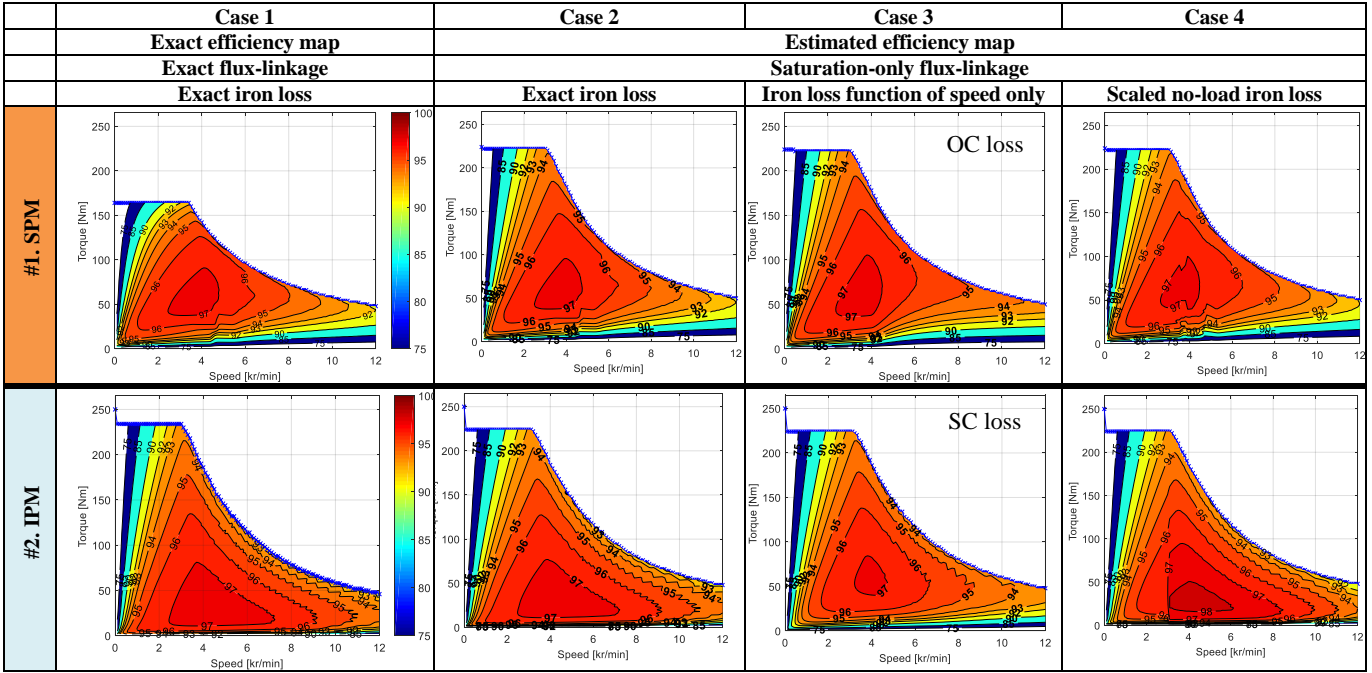|	Case 1	Case 2	Case 3	Case 4
	Exact efficiency map	Estimated efficiency map		
	Exact flux-linkage	Saturation-only flux-linkage		
	Exact iron loss	Exact iron loss	Iron loss function of speed only	Scaled no-load iron loss
#1. SPM			OC loss	
#2. IPM			SC loss	

Fig. 10 Comparison of exact and estimated efficiency maps for SPM and IPM machines.

produces a discontinuity in the efficiency contours at rated speed.

VII. VALIDATING THE FITTING FUNCTIONS

To validate the proposed loss fitting method, it was tested on two other machines as shown in Fig. 11 where the first row shows the machine cross-sections. The first and third columns show the previous SPM (Machine #1) and IPM (Machine #2) designs.

The second column shows the results for a spoke-type design (Machine #3) with two radial magnets per pole that was designed as a fixed-speed AC generator [16]. Though the spoke designs are strictly interior PM machines, this particular design uses large rare-earth magnets and is effectively a non-salient machine and hence considered a SPM design. It provides a useful contrast to the 50kW SPM design due to its different rotor geometry and stator winding arrangement (distributed versus concentrated). It has been constructed and its rated performance matches well with the FE predictions [16].

The fourth column shows the results for a 10kW IPM (Machine #4) [13]. Compared to the 50kW IPM machine this uses a three-barrier rather than a four-barrier rotor and ferrite rather than rare-earth magnets. Thus of the four machines, there are two which are non-salient and two which are salient, and one with concentrated windings and three with distributed windings.

The second and third rows show the fitting functions for the ratio of iron loss to no-load iron loss as a function of load for the constant torque and constant power regions. The scaling factors and exponents for the loss fitting functions for the four machines are summarized in Table II.

In Fig. 11, the second row compares the normalized iron loss in the constant torque region as a function of T^4 and $\sqrt{T}$ for the SPM and IPM machines, respectively. While the SPM

results show significant variation with speed (lines show significant scatter), the IPM results show little speed variation (lines are tightly grouped) and intriguingly similar behaviour for the two IPM machines.

The third row compares the losses in the constant power region. For the two SPM machines the iron losses fit reasonably to a function of P^4 while for the two IPMs functions of P^2 and P give reasonable fits.

The estimated efficiency map using the above iron loss fitting functions is shown in the fourth row and compared with the exact efficiency map in the fifth (last) row. To eliminate the effect of flux-linkage estimation errors, the detailed cross-saturation model is used when estimating the efficiency map for all four machines.

In comparing the estimated and exact efficiency maps, it was found that the proposed modelling approach gave accurate results for the two SPM machines in terms of the shape of the contours and the location and value of the peak efficiency. For the IPM machines though the modelling approach gave a reasonable prediction for the general shape, for machine #2 there was a 1% error in peak efficiency and for machine #4 there was an significant error in the location of the peak efficiency point.

Table II shows strong similarities between the values of the scaling factors and exponents for the two SPM machines and the two IPM machines. The largest difference in the scaling factors for the iron loss was found for the IPM machines in the constant torque region. As far as efficiency map prediction is concerned this is less important than the constant power region as the iron losses are generally smaller than the copper losses in constant torque region.

The only difference in the exponents of the iron loss fitting function was in the constant power region for the IPM machines

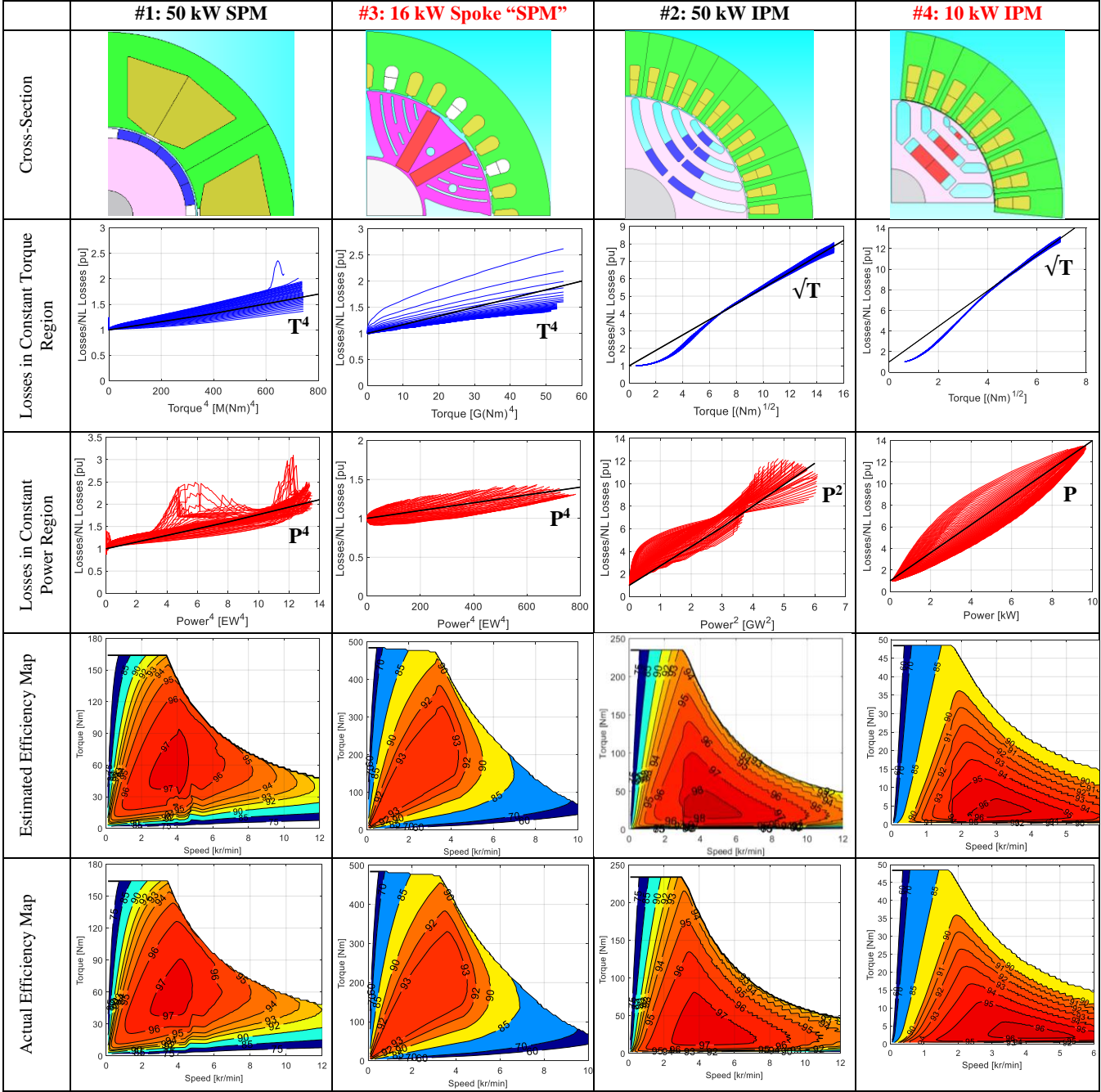|	**#1: 50 kW SPM**	**#3: 16 kW Spoke "SPM"**	**#2: 50 kW IPM**	**#4: 10 kW IPM**
Cross-Section				
Losses in Constant Torque Region				
Losses in Constant Power Region				
Estimated Efficiency Map				
Actual Efficiency Map				

Fig. 11 Comparison of the fitting of the iron loss in the constant torque and constant power regions and the estimated and actual efficiency maps.

where machine #2 had a fitting function of P^2 while machine #4 had a fitting function of P. The effect of using a fitting function of P^2 for machine #4 was investigated in Fig. 12. Interesting while the fitting function does not seem to match the iron loss as well, it produces an efficiency map which is much closer in shape to the exact efficiency map though with an approximately 1% error in the value of the peak efficiency.

The consistency of the above results for each machine type show the proposed loss fitting approach has potential. Areas for further work include: developing models which explain its theoretical foundations, examining a wider range of machines and validating it experimentally.

It is also important to note that the above analysis was performed with FE results without any mechanical loss components. Experimental data would include mechanical losses and the effect of this on the proposed fitting function approach also needs investigation.
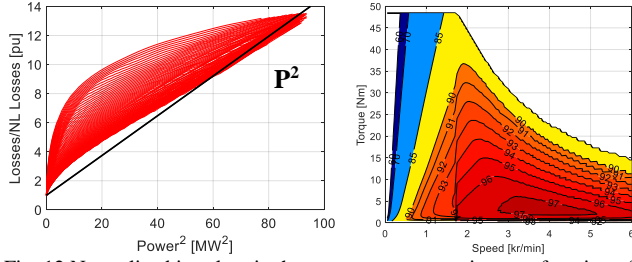
Fig. 12 Normalized iron loss in the constant power region as a function of power and resultant efficiency map for the new IPM motor.

Table III. Curve-Fit Parameters for No-Load Iron Loss.

	Constant Torque K_T, n_T		Constant Power K_P, n_P		Winding Type
	K	n	K	n	
#1: SPM (50 kW)	1.7	4	2.1	4	Concentrated
#3: SPM (16 kW)	1.4	4	2	4	Distributed
#2: IPM (50 kW)	8	0.5	12	2	Distributed
#4: IPM (10 kW)	14	0.5	13	1	Distributed

VIII.   Conclusions

This paper investigated estimating the efficiency map of an electric machine based on limited flux-linkage and iron loss data. The results are examined using detailed finite-element data from 50-kW surface PM (SPM) and interior PM (IPM) machines.

Using saturation-only flux-linkage results affects the estimation of the torque-speed capability envelope in the constant torque region and also the stator copper losses. It was found that the SPM machine had significant cross-saturation and thus showed substantial errors in the constant torque when using the saturation only model while the IPM had little cross-saturation and thus showed good results.

The iron loss at maximum efficiency is a function of both torque and speed. Using iron loss data as only a function of speed was found to give limited accuracy in the estimation of the efficiency map. An improved approach was proposed based on scaling the no-load iron loss data using a fitting function consisting of a scaling factor and a power law variation with load torque or power. Results were presented for two SPM and two IPM machines. It was found that the scaling factors and exponents for the two SPM machines and the two IPM machines showed good correspondence which is a promising indication of the validity of the proposed approach.

Proposed further work includes investigating the theoretical basis for the fitting functions and validation both for a wider range of machine types as well as experimentally.

REFERENCES

[1] M. Ferrari, N. Bianchi, A. Doria, and E. Fornasiero, "Design of synchronous reluctance motor for hybrid electric vehicles," *IEEE Transactions on Industry Applications,* vol. 51, no. 4, pp. 3030-3040, 2015.

[2] M. Takeno, A. Chiba, N. Hoshi, S. Ogasawara, M. Takemoto, and M. A. Rahman, "Test results and torque improvement of the 50-kW switched reluctance motor designed for hybrid electric vehicles," *IEEE Transactions on Industry Applications,* vol. 48, no. 4, pp. 1327-1334, 2012.

[3] T. Kato, M. Minowa, H. Hijikata, K. Akatsu, and R. D. Lorenz, "Design methodology for variable leakage flux IPM for automobile traction drives," *IEEE Transactions on Industry Applications,* vol. 51, no. 5, pp. 3811-3821, 2015.

[4] S. A. Odhano, R. Bojoi, A. Boglietti, Ş. G. Roşu, and G. Griva, "Maximum efficiency per torque direct flux vector control of induction motor drives," *IEEE transactions on Industry Applications,* vol. 51, no. 6, pp. 4415-4424, 2015.

[5] E. Armando, A. Boglietti, and R. Bojoi, "Electrical drives measurements and testing: Past, Present and Future," *IEEE Energy Conversion Congress and Exposition (ECCE),* 2018.

[6] A. Mahmoudi, W. L. Soong, G. Pellegrino, and E. Armando, "Efficiency maps of electrical machines," in *2015 IEEE Energy Conversion Congress and Exposition (ECCE)*, 2015: IEEE, pp. 2791-2799.

[7] A. Brune, P. Dück, B. Ponick, A. Kock, and M. Gröninger, "Evaluation of an efficiency-optimized calculation of PM synchronous machines' operating range using time-saving numerical and analytical coupling," in *Vehicle Power and Propulsion Conference (VPPC), 2012 IEEE*, 2012: IEEE, pp. 32-35.

[8] S. Stipetic and J. Goss, "Calculation of efficiency maps using scalable saturated flux-linkage and loss model of a synchronous motor," in *Electrical Machines (ICEM), 2016 XXII International Conference on*, 2016: IEEE, pp. 1380-1386.

[9] J. Goss, P. Mellor, R. Wrobel, D. Staton, and M. Popescu, "The design of AC permanent magnet motors for electric vehicles: A computationally efficient model of the operational envelope," 2012.

[10] S. Stipetic, J. Goss, D. Zarko, and M. Popescu, "Calculation of Efficiency Maps Using a Scalable Saturated Model of Synchronous Permanent Magnet Machines," *IEEE Transactions on Industry Applications,* vol. 54, no. 5, pp. 4257-4267, 2018.

[11] G. Heins, D. M. Ionel, D. Patterson, S. Stretz, and M. Thiele, "Combined experimental and numerical method for loss separation in permanent-magnet brushless machines," *IEEE Transactions on Industry Applications,* vol. 52, no. 2, pp. 1405-1412, 2015.

[12] A. Mahmoudi, W. Soong, G. Pellegrino, and E. Armando, "Loss Function Modeling of Efficiency Maps of Electrical Machines," *IEEE Transactions on Industry Applications,* 2017.

[13] S. Kahourzade, A. Mahmoudi, W. L. Soong, N. Ertugrul, and G. Pellegrino, "Estimation of PM Machine Efficiency Maps from Limited Experimental Data," in *2018 IEEE Energy Conversion Congress and Exposition (ECCE)*, 2018: IEEE, pp. 4315-4322.

[14] C. Lu, S. Ferrari, and G. Pellegrino, "Two design procedures for PM synchronous machines for electric powertrains," *IEEE Transactions on Transportation Electrification,* vol. 3, no. 1, pp. 98-107, 2017.

[15] A. M. El-Refaie, T. M. Jahns, P. B. Reddy, and J. W. McKeever, "Modified vector control algorithm for increasing partial-load efficiency of fractional-slot concentrated-winding surface PM machines," *IEEE Transactions on Industry Applications,* vol. 44, no. 5, pp. 1543-1551, 2008.

[16] W. L. Soong, S. Kahourzade, C.-Z. Liaw, and P. Lillington, "Interior PM generator for portable AC generator sets," *IEEE Transactions on Industry Applications,* vol. 52, no. 2, pp. 1340-1349, 2015.